

Flexoelectricity and Charge Separation in Carbon Nanotubes

Vasilii I. Artyukhov, Sunny Gupta, Alex Kutana, and Boris I. Yakobson*

Cite This: *Nano Lett.* 2020, 20, 3240–3246

Read Online

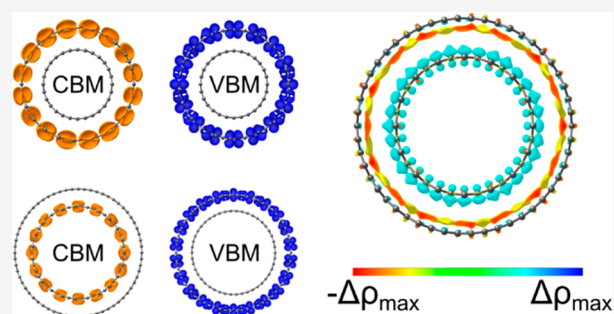
ACCESS |

Metrics & More

Article Recommendations

ABSTRACT: The effect of flexoelectric voltage on the electronic and optical properties of single- and double-wall carbon nanotubes is evaluated by the first-principles calculations. The voltage between the inner channel of curved sp^2 carbon nanostructures and their surroundings scales linearly with nanotube wall curvature and can be boosted/reversed by appropriate outer wall functionalization. We predict and verify computationally that in double-wall nanotubes, flexoelectricity causes a straddling to staggered band gap transition. Accurate band structure calculations taking into account quasiparticle corrections and excitonic effects lead to an estimated critical diameter of ~ 24 Å for this transition. Double-wall nanotubes above this diameter have staggered band alignment and could be potentially used for charge separation in photovoltaic devices.

KEYWORDS: excitonic photovoltaics, 1D van der Waals heterostructure, curvature effects, cylindrical double layer, staggered band alignment, many body effects



Carbon nanotubes have been long envisaged as a replacement of the current silicon-based technology and posed for use in future nanoscale devices and applications. They are presently seen as one of the main contenders to become the next key electronic material after silicon.^{1,2} Among many possible potential applications of carbon nanotubes, one is for current generation in photovoltaic devices. At the moment, carbon nanotubes have been already utilized in photovoltaic devices, albeit in auxiliary roles, for example, for improving charge separation and photocurrent generation³ or as a material for counter electrode⁴ in dye-sensitized excitonic solar cells. While these applications demonstrate their versatility as device components, the use of carbon nanotubes as an active medium for photovoltaic charge separation has not been considered yet to the best of our knowledge. The important condition of staggered band alignment to obtain the interwall charge transfer state seems not to be satisfied in double-wall carbon nanotubes (DWCNT). Here we consider theoretically the possibility of charge separation using DWCNT as an active medium and show that the straddling (type I) to staggered (type II) band gap transition occurs in DWCNT as their diameter increases. We identify flexoelectric voltage as one of the key factors responsible for the creation of staggered band alignment in DWCNT, suggesting new potential applications in charge separation devices.

In planar graphene, the charge density of carbon p orbitals is mirror-symmetric with respect to the atomic plane, as illustrated in Figure 1a. When the graphene sheet is rolled to form a nanotube, the curvature breaks the mirror symmetry. As

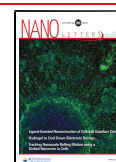
a result, π -electron density is “expelled” outward, creating a flexoelectric local dipole moment in the direction of, and proportional to, the curvature^{5,6,7} (Figure 1b). In the nanotube geometry, this dipole moment acts as a cylindrical double layer. The flexoelectric voltage V_{flex} between nanotube exterior and inner channel is proportional to the density of dipole, and it follows that $V_{\text{flex}} = V_0/D$ where D is the nanotube diameter and V_0 is a constant determined by flexoelectric polarizability of graphene.⁵ To our knowledge, this effect has not been utilized before, and in this work we confirm it with first-principles calculations and explore its physical consequences.

We begin by verifying the existence and studying the scaling of the flexoelectric voltage in single-wall carbon nanotubes (SWCNT). Figure 1c shows density functional theory (DFT) calculations for a series of SWCNT (black crosses) containing both zigzag and armchair tubes. The shown values are the electrostatic potential difference between the tube axis and outside the tube. The potential distributions featured distinctive uniform plateaus both in the outside region as well as, except for a few of the thinnest tubes, inside channel, clearly proving that the tube wall does act like a cylindrical capacitor. The black line in Figure 1c is a linear fit to the data.

Received: December 30, 2019

Revised: March 6, 2020

Published: March 10, 2020



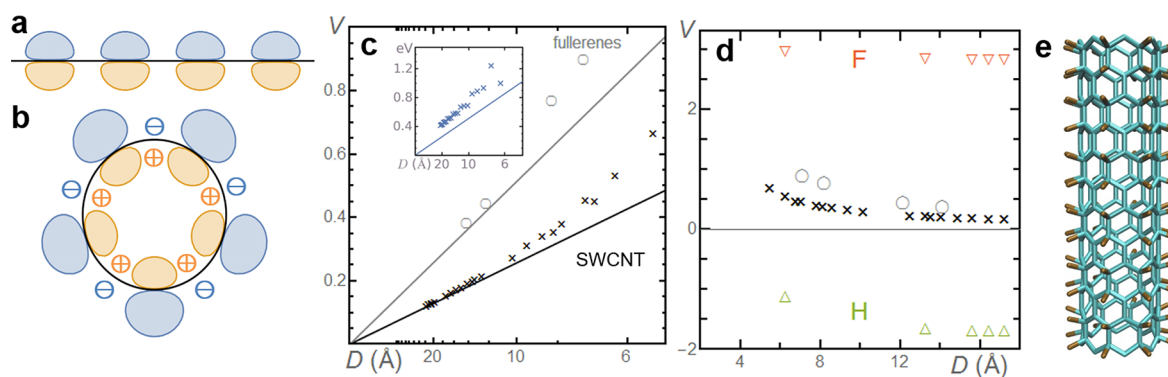


Figure 1. Flexoelectricity in sp^2 carbon. The symmetry of π -orbitals in graphene (a) is broken in nanotubes by their curvature, displacing electron density outward and creating a potential difference across the wall (b). (c) DFT data for voltage versus inverse diameter for (black crosses) nanotubes and (gray circles) fullerenes. The black line is a linear fit $V_{\text{flex}}(1/D)$ to large-diameter nanotubes, and the gray line is the same fit multiplied by 2 (corresponding to larger curvature of fullerenes). The inset in (c) shows the DFT charge inversion energy (Li^+ out, F^- in vs F^- out, Li^+ in); the line is the “theoretical” value, $2V_{\text{flex}}(1/D)$. (d) Tuning voltage with covalent functionalization. Decorating nanotube walls with electronegative (electropositive) species creates bond dipoles that induce a positive (negative) voltage across the nanotube wall. Crosses and circles correspond to flexoelectric voltages in (c). (e) Panel illustrates a (8, 0) carbon nanotube fluorinated to C_2F stoichiometry.

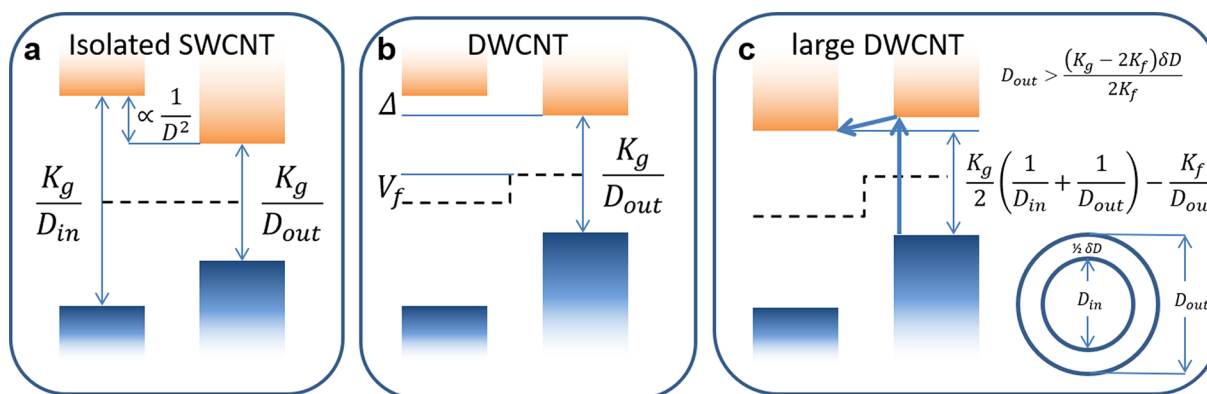


Figure 2. Schematic model for band alignment in double-wall nanotubes. (a) The band gaps of individual isolated walls are inversely proportional to their diameters, and the offset between the conduction bands is inverse-quadratic in diameter. In the DWCNT geometry, (b), this offset is reduced by the flexoelectric voltage, scaling inversely with the diameter. For sufficiently large DWCNT (c), the voltage exceeds the offset, resulting in a staggered-gap electronic structure and a charge-transfer excited state below the optical gap of the outer wall.

Tubes with diameter below ~ 10 Å were excluded from fitting, as the flexoelectric dipole scales superlinearly at high curvature.^{5,6} The equation for the fit is $2.56 \text{ eV}/D[\text{Å}]$. We also calculated flexoelectric voltages for fullerenes, shown with gray circles. The gray line is drawn at a slope of $5.12 \text{ eV}/D[\text{Å}]$, that is, twice of that for the nanotubes and represents the theoretical prediction for fullerenes based on the nanotube fit since the curvature of a sphere is twice that of a same-diameter cylinder. Overall we see good agreement between calculations and analytical predictions.

As an additional test, we have compared the energies of SWCNT with Li^+ and F^- ions inside and outside the nanotube, respectively, and with ion positions exchanged. The energy difference upon such charge inversion (crosses in Figure 1c inset) is somewhat above the “naïve” predicted value of $2V_{\text{flex}}$ shown with the blue line, perhaps due to the effects of π -system polarization, but clearly follows a decreasing trend with voltage as expected.

Flexoelectricity of sp^2 carbon is a remarkable but also fairly subtle effect. The absolute values of flexoelectric voltage of up to 600–800 meV (Figure 1c), however impressive for a nominally apolar material, may be insufficient for some applications. It may thus be desirable to boost and/or change

the sign of the voltage across nanotube walls. We next discuss a strategy to accomplish that via outer wall functionalization. A natural way of inducing dipoles perpendicular to the nanotube surface is by introducing appropriately oriented polar bonds. Carbon nanotubes have long been known to be easily fluorinated up to the C_2F composition.^{8,9} With fluorine being strongly electronegative, it is natural to assume that fluorination should boost the voltage between the inner nanotube channel and the outside. Indeed, our DFT calculations yield voltages of C_2F nanotubes of almost 3 V (Figure 1d, red down triangles, with the structural model shown in Figure 1e). Conversely, replacing fluorine with hydrogen, which is electropositive with respect to carbon, reverses the sign of bond dipole, producing voltages of up to -2 V (Figure 1d, green up triangles). Thus, although functionalization could strongly perturb the electronic properties of nanotubes, it may be a very powerful way of inducing voltage for certain applications (such as the above-mentioned ion capture or exchange).

Thus, we see that the expected flexoelectric voltage is real, and many interesting applications can be imagined for it. The energetic preference for negative (positive) ions inside (outside) may invite ion-exchange or water desalination uses.

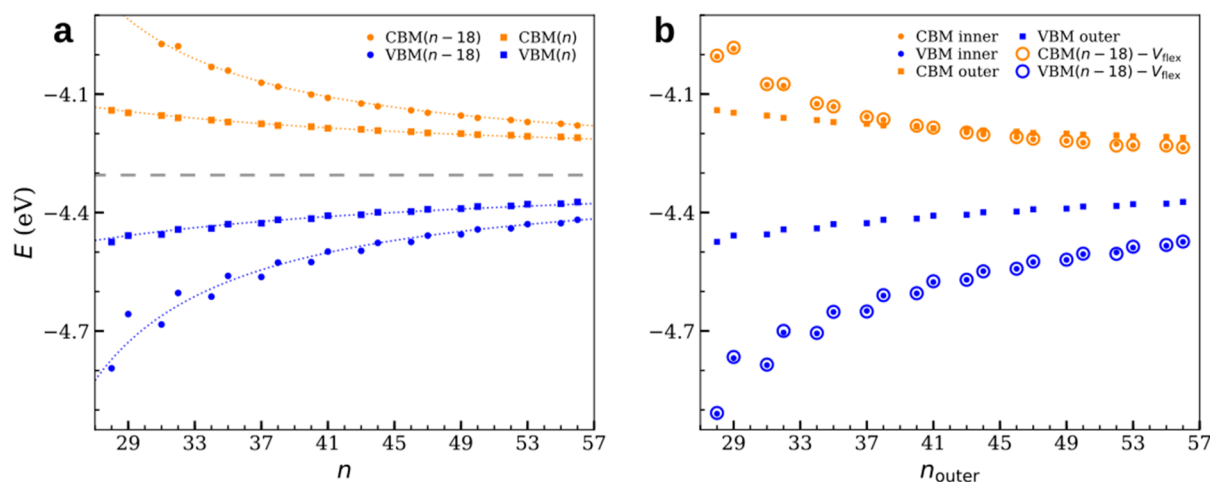


Figure 3. Alignment of Kohn–Sham bands in noninteracting double-wall nanotubes. (a) The band gaps of individual isolated walls, represented by SWCNT, are inversely proportional to their diameters, yielding straddling (type I) band alignment. (b) In noninteracting DWCNT, flexoelectric voltage of the outer wall yields staggered (type II) bands in DWCNTs after a threshold diameter $n = 40$.

From the chemical standpoint, the inner channel is a (Lewis) acidic environment, suggesting novel redox chemistry possibilities. Setting the above directions aside for future study, here we focus on a third possibility: flexoelectrically driven charge carrier separation in semiconducting double-wall nanotubes.

The physical insight behind charge separation possibility is illustrated in Figure 2. From here on, we will only discuss semiconducting tubes. In DWCNT, the diameter difference δD between inner and outer walls is approximately constant and close to twice the interlayer spacing in graphite ($\delta D \approx 6.8 \text{ \AA}$). The optimum interwall distance of about 3.4 \AA corresponds to a tube index difference of 9. The band gap of SWCNT is inversely proportional to the diameter, $E_g = K_g/D^9$, and in isolation the two walls of a DWCNT can be thought of as simply two materials whose band gaps differ only due to the difference in their diameter, yielding straddling (type I) band alignment, as shown in Figure 2a. The conduction band offset scales asymptotically as inverse-square diameter, $1/(D_{\text{out}} - \delta D) - 1/D_{\text{out}} \sim 1/D_{\text{out}}^2$ in this case. But when the inner wall is placed inside the outer one, the flexoelectric voltage of the outer wall shifts the band structure of the inner wall down by, based on the discussion above, $V_{\text{flex}} \sim 1/D_{\text{out}}$, as illustrated in Figure 2b. The shift creates a staggered (type II) band alignment (Figure 2c), with VBM on the outer tube and CBM on the inner. This situation can be realized in noninteracting tubes, for example, in a hypothetical $(n-18,0)@(n,0)$ system where the interwall distance is doubled compared to the normal DWCNT. The positions of the Kohn–Sham valence band maxima (VBM) and conduction band minima (CBM) of $(n-18,0)$ and $(n,0)$ SWCNT as well as their Fermi levels as a function of n yielding straddling band alignment is shown in Figure 3a. We verified with a DFT calculation that when the inner wall is placed inside the outer one, the flexoelectric voltage of the outer wall shifts the band structure of the inner wall down by V_{flex} . The shift creates a staggered band alignment with VBM on the outer tube and CBM on the inner after a threshold diameter of $n = 40$, as can be seen from Figure 3b. The bands of the isolated tubes are also plotted in Figure 3b, with shift of $-V_{\text{flex}}$ applied, showing that the model describes the $(n-18,0)@(n,0)$ tubes well. This noninteracting case can, for instance, be achieved if one separates the inner

and outer tube by growing a *h*-BN tube in between, thereby isolating the two tubes.

The band offset is smaller in $(n-9,0)@(n,0)$ tubes, and using the above model the band crossing would occur at $n \sim 20$. In reality for $(n-9,0)@(n,0)$ systems, however, this simple picture is altered due to the interwall interaction, as can be seen from Figure 4a, which shows the calculated band edge positions in actual DWCNT. The most important difference with the model neglecting interwall interactions is the shift of the threshold diameter at which the crossing of the conduction bands located on different walls takes place toward larger n .

Above this threshold diameter, the flexoelectric voltage and interwall interactions convert the normal straddling-gap band alignment of Figure 4a into a staggered-gap system. We verified the charge transfer state by plotting the spatial distribution of the band edge states in a $(23,0)@(32,0)$ DWCNT, as shown in Figure 4b, where one can see that the VBM is mainly located on the outer tube and the CBM on the inner one. In contrast, at small diameters band edges are mostly derived from the outer tube, as seen in Figure 4b, showing $(14,0)@(23,0)$. The DWCNT with large diameters are of less practical interest as they exhibit a collapsed metastable state at $D > 27 \text{ \AA}$ and become fully collapsed at $D > 56 \text{ \AA}$.¹¹ The difference between interacting and noninteracting tubes is due to interwall coupling. We find that in $(n-9,0)@(n,0)$ systems there is significant charge transfer from outer tube to inner tube due to hybridization of orbitals located on different walls (Figure 4c). The inner tube is negatively charged compared to the outer tube and the system again behaves as a cylindrical capacitor. But now, the electrostatic potential developed due to the charge transfer dipole counteracts the effect of the flexoelectric voltage. We calculated this counteracting voltage (Figure 4d) and name it V_{hyb} , that is, voltage developed due to orbital hybridization interactions between the tubes. A good fit of V_{hyb} is obtained with the analytical formula for potential difference in a cylindrical capacitor, as shown in Figure 4d. The nature of the hybridization between the electronic states of the two tubes is similar to interactions in bilayer graphene but with a net charge transfer due to wall curvature. The charge transfer dipole counteracts the effect of the flexoelectric voltage on the band edge positions and a staggered band alignment is obtained above a threshold diameter. The $(n,0)@(m,0)$

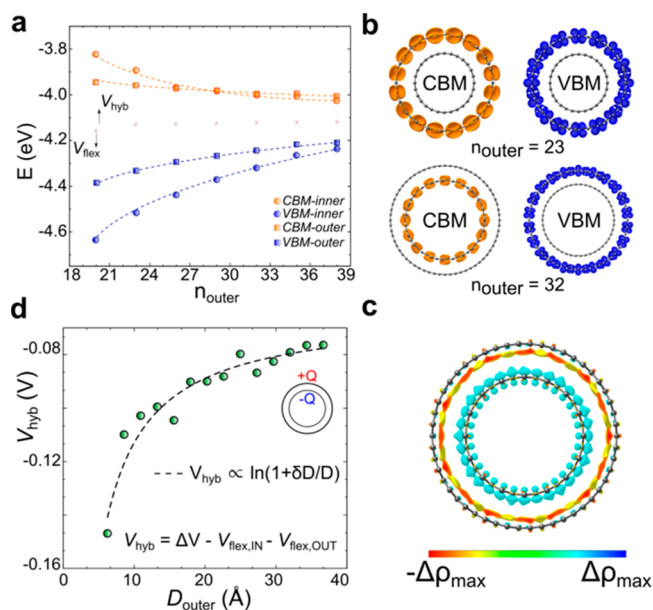


Figure 4. Charge transfer and band alignment in double wall nanotubes. (a) In interacting DWCNT, staggered-gap electronic structure and a charge-transfer excited state below the optical gap exists in sufficiently large DWCNT. (b) Band decomposed charge density showing that the CBM and VBM states are localized on the outer tube in (14,0)@(23,0) DWCNT, whereas in (23,0)@(32,0) DWCNT the CBM is localized on the inner tube and VBM on the outer, thereby forming a staggered band alignment. (c) Isocharge plot showing significant charge transfer from the outer tube to the inner tube. (d) The charge transfer results in a cylindrical capacitor with the inner tube being negatively charged. The voltage difference (V_{hyb}) developed due to the charge transfer is plotted as a function of the outer tube diameter and a good fit with the analytical formula is obtained. ΔV is the potential difference between the inside and outside of the DWCNT, whereas V_{flex} is the flexoelectric voltage resulting from isolated tubes.

DWCNTs considered in our study have weak intertube coupling and V_{hybrid} can be treated as a correction to V_{flex} . One should keep in mind though that in the case of special incommensurate chiral DWCNTs^{12,13} with strong interlayer coupling the simple model of type-I or type-II band alignment might not be applicable. In particular, the special localized insulating coupling conditions arise in the near zigzag–zigzag DWCNTs but not in pure zigzag considered here. In such DWCNTs, including a BN nanotube as a spacer can be used to reduce interlayer coupling but it might also weaken the charge transfer rate and further optimization would be required.

To detect the charge-transfer state, we have performed extensive calculations of electronic and optical spectra beyond the DFT level for a range of semiconducting zigzag SWCNT and DWCNT with diameters up to 25 Å, corresponding to the (32,0) outer nanotube, for DWCNT ranging from (7,0)@(16,0) to (23,0)@(32,0). Since quantitative position of the crossover is sensitive to band gap, DFT was followed by G_0W_0 ¹⁴ calculations to correct for gap underestimation, which was in turn followed by Bethe–Salpeter equation (BSE) calculations to account for electron–hole interactions as well as to determine optical strengths of transitions.

The main result of this work is presented in Figure 5. Blue circles and green triangles represent G_0W_0 quasiparticle band gaps of SWCNT and DWCNT, respectively. For DWCNT, the size is defined by the diameter of the outer wall. In the middle

part of the plot, the points are seen to be converging toward each other with DWCNT gaps being slightly larger. The difference can be attributed to interwall screening,¹⁵ similar, for example, to substrate screening effects in transition metal chalcogenides on graphene.¹⁶ However, for the two largest tubes, (31,0) and (32,0), the DWCNT gap is smaller than that of the SWCNT, indicating the transition to staggered gap.

The transition is even more obvious from the analysis of optical spectra of DWCNT. Red diamonds in Figure 5 denote the optical gaps, lowest-energy bright transitions, of DWCNT. These are due to the A_{11} exciton of the outer wall, and nearly coincide in energy with the corresponding transitions in SWCNT, shown with black squares. At the same time, DWCNT optical spectra contain a dark state formed by the valence and conduction bands located on different walls, shown by orange triangles. For the diameters larger than 24 Å, this charge-transfer state lies below the optical gap, providing a driving force for carrier splitting. Our calculations yield a 10^3 – 10^5 lower brightness compared to the outer-wall exciton, which is expected from the small overlap of electron and hole wave functions localized on different walls.

Thus, our calculations confirm the prediction of the dark charge-transfer state in large-diameter DWCNT. In addition to the calculations reported in Figure 5, we analyzed pure and hybrid DFT calculations (as well as a set of G_0W_0 calculations with coarser Brillouin zone samplings but higher basis set cutoffs), all of which predicted the transition to happen at a somewhat lower diameter ~ 23 Å corresponding to the (29,0) outer tube. In practice, we expect the transition not to be perfectly sharp but somewhat diffuse with both straddling- and staggered-gap tubes in the immediate vicinity of the critical diameter since there are some variations of SWCNT band gaps around the $1/R$ asymptotic. These manifest themselves in Figure 5 as the two “families” of zigzag tubes.

So far we have not mentioned the low-lying charge-transfer state seen in Figure 5 on the left (below 14 Å diameter). While it is of little practical importance, it warrants a brief digression to prevent confusion. This point represents the (8,0)@(17,0) system in which the inner tube is extremely narrow. In such thin zigzag tubes, the band gap is formed by a single-degenerate state that is derived from the M point of the graphene Brillouin zone. Normally, this state lies deep in the conduction band but is sensitive to the extreme wall curvature,¹⁷ causing the band to be below the two K point states that normally comprise the edge of the conduction band.¹⁰ Because of this effect, the band gaps of (8,0) and (17,0) tubes are approximately equal and thus even a slightest bias can create a staggered band alignment. For the (7,0)@(16,0) system, the situation is even more extreme with the band gap of the inner wall so small that the band gap is completely broken in DWCNT. Both examples were “accidentally” discovered in DFT calculations that employed zigzag tubes as a computationally efficient model of generic semiconducting tubes.¹⁸ However, it is important to remember that the effect that causes this conduction band crossover applies exclusively to small-diameter zigzag inner tubes¹⁷ and, indeed, there are only two such tubes that are semiconducting: (7,0) and (8,0). In stark contrast, the general flexoelectric effect discovered in this work should apply universally to all semiconducting DWCNT above the critical diameter.

The present work adds flexoelectric voltage to the long list of outstanding properties of carbon nanotubes. While we are not aware of any direct detection in nanotubes, C_{60} has been

reported to have a peculiar delocalized s -type anionic state¹⁹ that implies existence of the flexoelectric potential well inside closed sp^2 -carbon shells. The charge separation predicted in DWCNTs will lead to a long exciton lifetime which is desirable in optoelectronics and photovoltaics. However, these excitons must be dissociated into free carriers for possible applications. To reduce the binding energy, the nanotubes can be embedded in a high dielectric medium. Since the exciton binding energy (E_B) in nanotubes scales²⁰ with the dielectric constant (ϵ) of the embedded medium as $E_B \propto \epsilon^{-1.4}$, a medium with $\epsilon > 27$ can reduce E_B by 2 orders of magnitude. A high dielectric constant oxide²¹ can thus be used as an embedding medium to reduce the binding energy of excitons in DWCNTs and thermal energy will be sufficient to dissociate them into free carriers

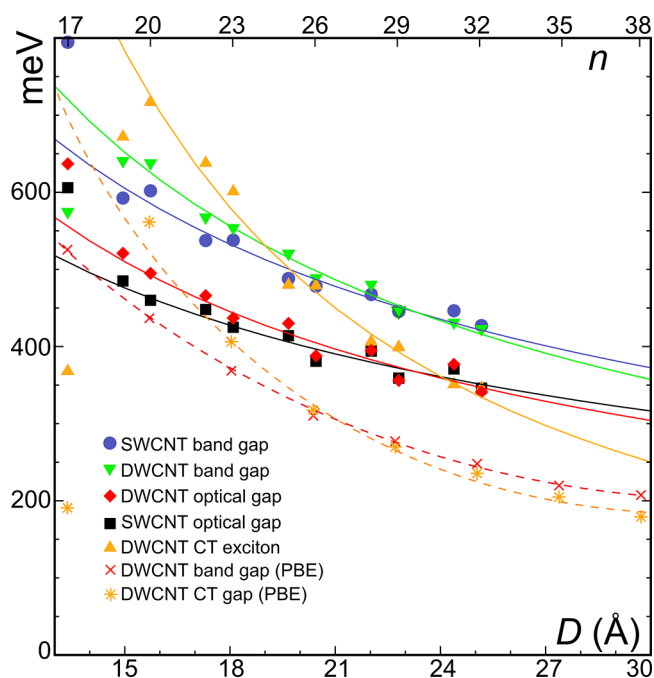


Figure 5. Excitations in single and double-wall nanotubes. Optical, fundamental, and Kohn–Sham band gaps are shown. For DWCNT, the diameter is that of the outer wall since it has a smaller band gap and therefore is responsible for low-lying excited states. The fundamental band gaps are calculated in the GW approximation. The optical gaps and charge-transfer exciton energies are computed using the Bethe–Salpeter equation on top of G_0W_0 .

required for photovoltaics. Even if the energies involved turn out to be below the most useful range for practical photovoltaic applications, this type of band structure may be useful for IR optoelectronic applications or observation of other interesting physical effects such as Coulomb drag or exciton condensation.^{22–24} In systems with spatially separated electrons and holes, the maximum energy gap Δ in the single-particle excitation spectrum is achieved when the interwall distance is smaller than exciton radius, potentially yielding measurable transition temperatures.²² DWCNT could thus hold promise for exhibiting exciton condensation. Single-DWCNT optical experiments with reliable wall type assignment have only recently become possible and are already yielding interesting information,²⁵ and recent progress in DWCNT synthesis and sorting²⁶ makes research into their optical properties especially timely. As a last note, we point out that boron nitride (BN) nanotubes can be considered an

intermediate case between pristine and functionalized nanotubes considered here, as the BN layer undergoes buckling upon bending with B^+ shifting inward relative to N^- ,²⁷ producing polarization without adsorption of extrinsic species. Nanotubes of other polar materials, especially those that already have out-of-plane bonds such as silica,^{28,29} could demonstrate an even stronger effect.

In summary, we predict and confirm with first-principles calculations the existence of a flexoelectric voltage between the inner channel of carbon nanotubes and the outside due to breaking of the π -orbital symmetry by wall curvature. The flexoelectric voltage in SWCNT may eventually find catalytic or ionic applications. DWCNT are even more promising: a simple model based on asymptotics of nanotube band gap and the flexoelectric voltage leads us to predict a transition from straddling to staggered band structure above a threshold diameter, above which the lowest excited state is a dark charge-transfer exciton. High-level first-principles calculations support this prediction and place the quantitative value of the diameter threshold at around 2.5 nm. We also demonstrate that adsorbing electronegative or electropositive atoms on the nanotube surface can create substantial voltages of either sign and up to 3 V in absolute magnitude. Besides carbon nanotubes, various aspects of present findings apply to other tubular systems, most notably, nanotubes of BN, MoS_2 , and so forth, or their coaxial hybrids with SWCNT or among themselves, similar to planar heterobilayers.²⁴

■ COMPUTATIONAL DETAILS

DFT calculations for Figures 1, 3 and 4 were performed using Quantum-ESPRESSO³⁰ with the PBE density functional,^{31,32} 48 k -points for Brillouin zone sampling, and 60 (70) Ry basis set cutoff for pure (functionalized) nanotubes. Calculations for Figure 5 were performed using VASP.^{33,34} Initial geometries were obtained by relaxation with the PBEsol functional³⁵ and a 400 eV plane-wave cutoff, followed by LDA+ G_0W_0 calculations with a 300 eV DFT cutoff and 75 eV GW cutoff, and 24 frequency-axis points. To ensure convergence of dielectric matrix, 48 k -points had to be used. BSE calculations were performed using 32 bands (16 in valence and conduction band each). Additional calculations of electronic structure were performed with the HSE hybrid functional^{36,37} with a 400 eV cutoff and 6 k -points. Additional G_0W_0 calculations were done with 250/150 DFT/GW cutoff, 48 frequency points, and 6 k -points. Projector-augmented wave basis sets were used throughout.^{38,39}

■ AUTHOR INFORMATION

Corresponding Author

Boris I. Yakobson – Department of Materials Science and NanoEngineering and Department of Chemistry, Rice University, Houston 77005, Texas, United States; Email: biy@rice.edu

Authors

Vasilii I. Artyukhov – Quantlab Financial, Houston, Texas 77046, United States; Department of Materials Science and NanoEngineering, Rice University, Houston 77005, Texas, United States

Sunny Gupta – Department of Materials Science and NanoEngineering, Rice University, Houston 77005, Texas, United States; orcid.org/0000-0001-5763-6411

Alex Kutana – Department of Materials Science and NanoEngineering, Rice University, Houston 77005, Texas, United States; orcid.org/0000-0001-6405-6466

Complete contact information is available at:
<https://pubs.acs.org/10.1021/acs.nanolett.9b05345>

Notes

The authors declare no competing financial interest.

ACKNOWLEDGMENTS

The authors acknowledge DoD HPCMP, and National Energy Research Scientific Computing Center (NERSC), a U.S. Department of Energy Office of Science User Facility for computational resources. Work was supported by the Army Research Office (W911NF-16-1-0255) and by the Robert Welch Foundation (C-1590).

REFERENCES

- (1) Shulaker, M. M.; Hills, G.; Patil, N.; Wei, H.; Chen, H.-Y.; Wong, H.-S. P.; Mitra, S. Carbon Nanotube Computer. *Nature* **2013**, *501* (7468), 526–530.
- (2) Cao, Q.; Han, S.-J.; Tersoff, J.; Franklin, A. D.; Zhu, Y.; Zhang, Z.; Tulevski, G. S.; Tang, J.; Haensch, W. End-Bonded Contacts for Carbon Nanotube Transistors with Low, Size-Independent Resistance. *Science* **2015**, *350* (6256), 68–72.
- (3) Brown, P.; Takechi, K.; Kamat, P. V. Single-Walled Carbon Nanotube Scaffolds for Dye-Sensitized Solar Cells. *J. Phys. Chem. C* **2008**, *112* (12), 4776–4782.
- (4) Park, J.-G.; Akhtar, M. S.; Li, Z. Y.; Cho, D.-S.; Lee, W.; Yang, O.-B. Application of Single Walled Carbon Nanotubes as Counter Electrode for Dye Sensitized Solar Cells. *Electrochim. Acta* **2012**, *85*, 600–604.
- (5) Dumitrică, T.; Landis, C. M.; Yakobson, B. I. Curvature-Induced Polarization in Carbon Nanoshells. *Chem. Phys. Lett.* **2002**, *360* (1–2), 182–188.
- (6) Kvashnin, A. G.; Sorokin, P. B.; Yakobson, B. I. Flexoelectricity in Carbon Nanostructures: Nanotubes, Fullerenes, and Nanocones. *J. Phys. Chem. Lett.* **2015**, *6* (14), 2740–2744.
- (7) Kutana, A.; Artyukhov, V. I.; Yakobson, B. I. In *APS March Meeting Abstracts*; 2015; <http://meetings.aps.org/Meeting/MAR15/Session/F34.2>
- (8) Mickelson, E. T.; Huffman, C. B.; Rinzler, A. G.; Smalley, R. E.; Hauge, R. H.; Margrave, J. L. Fluorination of Single-Wall Carbon Nanotubes. *Chem. Phys. Lett.* **1998**, *296* (1–2), 188–194.
- (9) Khabashesku, V. N.; Billups, W. E.; Margrave, J. L. Fluorination of Single-Wall Carbon Nanotubes and Subsequent Derivatization Reactions. *Acc. Chem. Res.* **2002**, *35* (12), 1087–1095.
- (10) Saito, R.; Fujita, M.; Dresselhaus, G.; Dresselhaus, M. S. Electronic Structure of Graphene Tubules Based on C60. *Phys. Rev. B: Condens. Matter Mater. Phys.* **1992**, *46* (3), 1804–1811.
- (11) Xiao, J.; Liu, B.; Huang, Y.; Zuo, J.; Hwang, K.-C.; Yu, M.-F. Collapse and Stability of Single- and Multi-Wall Carbon Nanotubes. *Nanotechnology* **2007**, *18* (39), 395703.
- (12) Koshino, M.; Moon, P.; Son, Y.-W. Incommensurate Double-Walled Carbon Nanotubes as One-Dimensional Moiré Crystals. *Phys. Rev. B: Condens. Matter Mater. Phys.* **2015**, *91* (3), No. 035405.
- (13) Zhao, S.; Moon, P.; Miyauchi, Y.; Matsuda, K.; Koshino, M.; Kitaura, R. Observation of Drastic Electronic Structure Change in One-Dimensional Moiré Crystals. 2019, *arXiv:1906.09421*.
- (14) Hybertsen, M. S.; Louie, S. G. Electron Correlation in Semiconductors and Insulators: Band Gaps and Quasiparticle Energies. *Phys. Rev. B: Condens. Matter Mater. Phys.* **1986**, *34* (8), 5390–5413.
- (15) Tomio, Y.; Suzuura, H.; Ando, T. Interwall Screening and Excitons in Double-Wall Carbon Nanotubes. *Phys. Rev. B: Condens. Matter Mater. Phys.* **2012**, *85* (8), No. 085411.
- (16) Ugeda, M. M.; Bradley, A. J.; Shi, S.-F.; da Jornada, F. H.; Zhang, Y.; Qiu, D. Y.; Ruan, W.; Mo, S.-K.; Hussain, Z.; Shen, Z.-X.; et al. Giant Bandgap Renormalization and Excitonic Effects in a Monolayer Transition Metal Dichalcogenide Semiconductor. *Nat. Mater.* **2014**, *13* (12), 1091–1095.
- (17) Blase, X.; Benedict, L. X.; Shirley, E. L.; Louie, S. G. Hybridization Effects and Metallicity in Small Radius Carbon Nanotubes. *Phys. Rev. Lett.* **1994**, *72* (12), 1878–1881.
- (18) Zólyomi, V.; Koltai, J.; Ruzsnyák, A.; Kürti, J.; Gali, Á.; Simon, F.; Kuzmany, H.; Szabados, A.; Surján, P. R. Intershell Interaction in Double Walled Carbon Nanotubes: Charge Transfer and Orbital Mixing. *Phys. Rev. B: Condens. Matter Mater. Phys.* **2008**, *77* (24), 245403.
- (19) Voora, V. K.; Cederbaum, L. S.; Jordan, K. D. Existence of a Correlation Bound S-Type Anion State of C60. *J. Phys. Chem. Lett.* **2013**, *4*, 849–853.
- (20) Perebeinos, V.; Tersoff, J.; Avouris, P. Scaling of Excitons in Carbon Nanotubes. *Phys. Rev. Lett.* **2004**, *92*, 257402.
- (21) Robertson, J. High Dielectric Constant Oxides. *Eur. Phys. J.: Appl. Phys.* **2004**, *28*, 265–291.
- (22) Lozovik, Y. E.; Yudson, V. Feasibility of Superfluidity of Paired Spatially Separated Electrons and Holes; a New Superconductivity Mechanism. *JETP Lett.* **1975**, *22* (11), 274–276.
- (23) Abergel, D. S. L. Excitonic Condensation in Spatially Separated One-Dimensional Systems. *Appl. Phys. Lett.* **2015**, *106*, 213103.
- (24) Gupta, S.; Kutana, A.; Yakobson, B. I. Hetero-Bilayers of 2D-Materials as a Platform for Excitonic Superfluidity. 2019, *arXiv:1908.07513*.
- (25) Liu, K.; Jin, C.; Hong, X.; Kim, J.; Zettl, A.; Wang, E.; Wang, F. Van der Waals-Coupled Electronic States in Incommensurate Double-Walled Carbon Nanotubes. *Nat. Phys.* **2014**, *10*, 737–742.
- (26) Loiseau, A.; Ghedjati, A.; Fossard, F.; Flahaut, E.; Laurent, J.-S. Structure and Sorting of DWNTs by Diameter and Helicity. In *NT14: The Fifteenth International Conference on the Science and Application of Nanotubes*; Los Angeles, CA, 2014.
- (27) Zhang, Z.; Guo, W.; Dai, Y. Stability and Electronic Properties of Small Boron Nitride Nanotubes. *J. Appl. Phys.* **2009**, *105* (8), No. 084312.
- (28) Chernozatonskii, L. A. A New Class of MO₂ Dioxide Nanotubes (M= Si, Ge, Sn, Pb) Composed of “Square” Lattices of Atoms: Their Structure and Energy Characteristics. *JETP Lett.* **2004**, *80* (10), 628–632.
- (29) Chernozatonskii, L. A.; Artyukhov, V. I.; Sorokin, P. B. Silica Nanotube Multi-Terminal Junctions as a Coating for Carbon Nanotube Junctions. *Phys. Rev. B: Condens. Matter Mater. Phys.* **2006**, *74* (4), No. 045402.
- (30) Giannozzi, P.; Baroni, S.; Bonini, N.; Calandra, M.; Car, R.; Cavazzoni, C.; Ceresoli, D.; Chiarotti, G. L.; Cococcioni, M.; Dabo, I.; et al. QUANTUM ESPRESSO: A Modular and Open-Source Software Project for Quantum Simulations of Materials. *J. Phys.: Condens. Matter* **2009**, *21* (39), 395502.
- (31) Perdew, J. P.; Burke, K.; Wang, Y. Generalized Gradient Approximation for the Exchange-Correlation Hole of a Many-Electron System. *Phys. Rev. B: Condens. Matter Mater. Phys.* **1996**, *54* (23), 16533–16539.
- (32) Perdew, J. P.; Burke, K.; Ernzerhof, M. Generalized Gradient Approximation Made Simple[*Phys. Rev. Lett.* **77**, 3865 (1996)]. *Phys. Rev. Lett.* **1997**, *78* (7), 1396.
- (33) Kresse, G.; Hafner, J. Ab Initio Molecular Dynamics for Liquid Metals. *Phys. Rev. B: Condens. Matter Mater. Phys.* **1993**, *47* (1), 558–561.
- (34) Kresse, G.; Furthmüller, J. Efficient Iterative Schemes for Ab Initio Total-Energy Calculations Using a Plane-Wave Basis Set. *Phys. Rev. B: Condens. Matter Mater. Phys.* **1996**, *54* (16), 11169–11186.
- (35) Perdew, J.; Ruzsinszky, A.; Csonka, G.; Vydrov, O.; Scuseria, G.; Constantin, L.; Zhou, X.; Burke, K. Restoring the Density-Gradient Expansion for Exchange in Solids and Surfaces. *Phys. Rev. Lett.* **2008**, *100* (13), 136406.

(36) Heyd, J.; Scuseria, G. E.; Ernzerhof, M. Hybrid Functionals Based on a Screened Coulomb Potential. *J. Chem. Phys.* **2003**, *118* (18), 8207–8215.

(37) Heyd, J.; Scuseria, G. E.; Ernzerhof, M. Erratum: “Hybrid Functionals Based on a Screened Coulomb Potential” [*J. Chem. Phys.* **118**, 8207 (2003)]. *J. Chem. Phys.* **2006**, *124* (21), 219906–219906–1.

(38) Blöchl, P. E. Projector Augmented-Wave Method. *Phys. Rev. B: Condens. Matter Mater. Phys.* **1994**, *50* (24), 17953.

(39) Kresse, G.; Joubert, D. From Ultrasoft Pseudopotentials to the Projector Augmented-Wave Method. *Phys. Rev. B: Condens. Matter Mater. Phys.* **1999**, *59* (3), 1758–1775.

(40) Xiang, R.; Inoue, T.; Zheng, Y.; Kumamoto, A.; Qian, Y.; Sato, Y.; Liu, M.; Tang, D.; Gokhale, D.; Guo, J.; Hisama, K. One-Dimensional van der Waals Heterostructures. *Science* **2020**, *367* (6477), 537–542.

(41) Gogotsi, Y.; Yakobson, B. I. Nested Hybrid Nanotubes. *Science* **2020**, *367* (6477), 506–507.

■ NOTE ADDED IN PROOF

During the peer review of the manuscript, a synthesis of hybrid nested (like SWCNT@BN@MoS₂) 1D van der Waals heterostructures was reported,⁴⁰ where the curvature of cylinders and the resulting band offsets, discussed above, must play significant role.⁴¹

■ NOTE ADDED AFTER ASAP PUBLICATION

Due to a production error, this paper was published ASAP on April 29, 2020, with incorrect affiliations attributed to Boris I. Yakobson and Vasilii I. Artyukhov. The corrected version was reposted on May 4, 2020.